Development of a New Type of Earthquake Energy-absorption Device

ZHU Huajia & SUN Yuping
Dept. of Architecture, Kobe University, Japan

FUJINAGA Takashi
RCUSS, Kobe University, Japan

TAKEUCHI Takashi
Dept. of Architecture, Kobe University, Japan

SUMMARY:
This paper presents a new kind of shear panel device with simple working mechanism and high cost performance. The proposed device consists of a steel panel sandwiched between two mortar plates wrapped with carbon fiber sheets (CF sheets) to confine the out-of-plane deflection caused by shear buckling of the steel panel. To investigate the hysteretic performances of the device, cyclical loading tests of small-scale specimens with different confinement conditions were conducted. The experimental results have indicated that the mortar plates and CF sheets can effectively confine the out-of-plane deflection and ensure sufficient energy absorption capacity. It has also been verified that the specimens with width-thickness ratio of about 55, thickness of mortar plate over 20mm, and 2 layers of CF sheet exhibited better hysteretic performances. In addition, the initial stiffness, strength and hysteretic loops can be simply and accurately evaluated by using several concise equations and the Skeleton-shift Model.

Keywords: Shear panel, Out-of-plane deflection, Mortar plate, Carbon fiber sheet, Confinement, Hysteretic performances

1. INTRODUCTION

As structure control systems, dampers play an important role to dissipate energy during large earthquakes in the energy based seismic response control design approaches (Akiyama et al. 1998) in Japan. Many kinds of hysteretic dampers such as steel shear damper have been studied experimentally and theoretically by Tanaka and Sasaki (1998), Tanaka et al. (1999), Ikarashi et al. (2007), and they have been successfully used in practical constructions for improving the ultimate resisting capacity of structures and reducing their damage under earthquake loading. However, most of these previous steel shear dampers cannot be simply designed, due to their complexity of working mechanism caused by welded stiffeners and ribs, and have low cost performance by using low yield point steel.

A new type of earthquake energy-absorption device with both simpler working mechanism and higher cost performance has been proposed by the authors. As shown in Fig. 1, the proposed device consists of a mild steel panel sandwiched between two pieces of mortar plates wrapped with carbon fiber sheets (CF sheets). The steel panel is expected to dissipate the earthquake energy by means of its pure shear deformation, which promises large energy dissipation capacity, while the mortar plates and CF sheets are used to confine the out-of-plane deformation of the steel panel caused by shear buckling.

In this research, small-scale specimens with different conditions are tested to investigate basic hysteretic properties of the proposed device, and the effectiveness of mortar plates and CF sheets as confinement of steel shear panel. Strength, stiffness and hysteresis modelling of the specimens are also evaluated and discussed to clarify convenience of the proposed device in practical use.

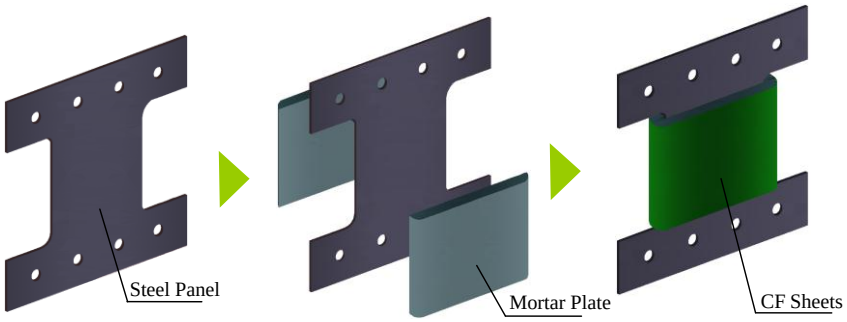

Figure 1. Concept of the proposed device

2. OUTLINE OF EXPERIMENT

2.1 Test Specimens

To investigate the basic hysteretic performances of the proposed device, eight 1/3-scale steel shear panel specimens were fabricated and tested under reversed cyclical lateral loading. All specimens consist of a steel panel, two pieces of mortar plates and CF sheets. The experimental variables among the tests are 1) the thickness of steel panel, 2) the thickness of the mortar plate, and 3) the number of layers of the CF sheet. Two types of thickness of the steel panel (2.3 and 3.2mm), three types of thickness of mortar plate (20, 30 and 40mm), and two types of number of layers of the CF sheet (1 and 2 layers) were adopted.

Steel panels of all eight specimens had square-shaped configuration (176mm×176mm, aspect ratio 1.0), and were made of conventional mild steel (JIS SS400). Mechanical properties of the steels are listed in Table 2.1. To reduce the stress concentration, the corners of steel panel were rounded to arc sharp with a radius of 20mm, and these panels are fastened between two L-shaped angle steel by high-strength bolts instead of being welded to the end plates. Material properties of mortar and CF sheet used are presented in Table 2.2. Non-shrinkage mortar was used in the tests for preventing cracks. In order to prevent stress concentration in CF sheet at the sharp corner, the external edges of each mortar plate had been rounded by grinding to achieve a radius of 20mm before it was wrapped by CF sheets. A minimum overlap length of CF sheet (50 mm) was provided in the tests. The dimensions of some specimens are shown in Fig. 2, and the details of all specimens are given in Table 2.3.

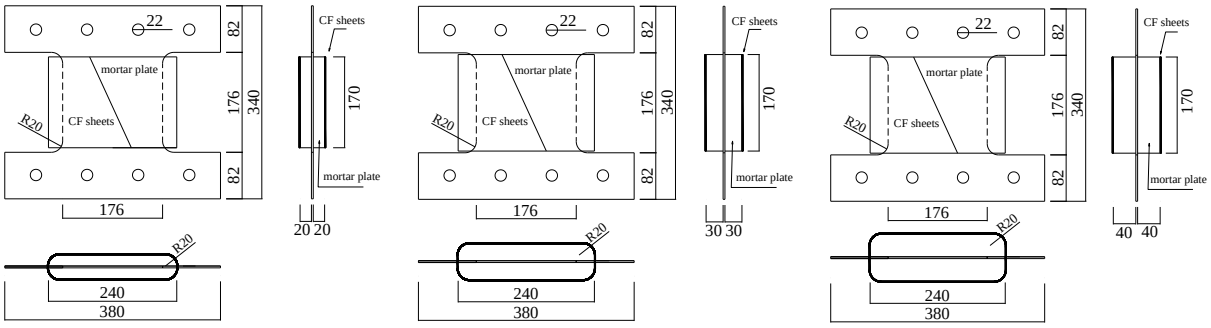

(a) PB77-M20 (b) PB77-M30 (c) PB77-M40

Figure 2. Examples of dimensions of test specimens (Unit: mm)

Table 2.1. Mechanical Properties of the Steel Panels

	Material	Thickness (mm)	Modulus of Elasticity (N/mm^2)	Yield Strength (N/mm^2)	Tensile Strength (N/mm^2)	Elongation (%)
PL2.3	JIS SS400	2.22	179000	281.3	431.8	37.5
PL3.2		3.06	193000	302.7	427.1	39.0

Table 2.2. Mechanical Properties of Mortar and Carbon Fiber Sheet

Mortar			Carbon Fiber Sheet			
Type	Design Strength (N/mm^2)	Modulus of Elasticity (N/mm^2)	Sheet Weight (g/cm^2)	Thickness (mm)	Tensile Strength (N/mm^2)	Modulus of Elasticity (N/mm^2)
Non-shrinkage	60	27000	300	0.167	3400	245000

Table 2.3. Details of the Specimens

Specimen	Steel Panel				Mortar Plate			CF Sheet
	Material	Width (mm)	Height (mm)	Width-thickness Ratio b/t	Width (mm)	Height (mm)	Thickness (mm)	Number of Layers
PB77-M20-1	PL2.3	176	176	77	240	170	20	1
PB55-M20-1	PL3.2			55				
PB77-M20	PL2.3			77				2
PB55-M20	PL3.2			55				
PB77-M30	PL2.3			77			30	
PB55-M30	PL3.2			55				
PB77-M40	PL2.3			77			40	
PB55-M40	PL3.2			55				

2.2 Testing Method and Measurements

The experimental apparatus used to apply the alternate cyclic load is shown in Fig. 3(a). The test specimen was installed between loading girder and foundation girder, and was fastened to them by high-strength bolts. The horizontal loading was applied to the top of the specimen via the loading girder by a horizontally placed 500kN hydraulic jack, and a pantograph was used to keep the loading girder moving horizontally. All specimens were free from axial stress and axial constraint. The magnitude of the horizontal load was measured by a load-cell built into the hydraulic jack, and the horizontal displacement of loading girder was measured by LVDTs installed on the loading girder. All tests were done under displacement control by computer and the loading history is shown in Fig. 3(b). Cyclical load repeated twice at the drift angle γ of 0.005rad and 0.01rad, and three times at each other large drift angle until the end of tests. The term "γ" in this paper represents drift angle of specimen, which is the horizontal displacement at the top of the specimen relative to its bottom divided by the height of steel panel (176mm).

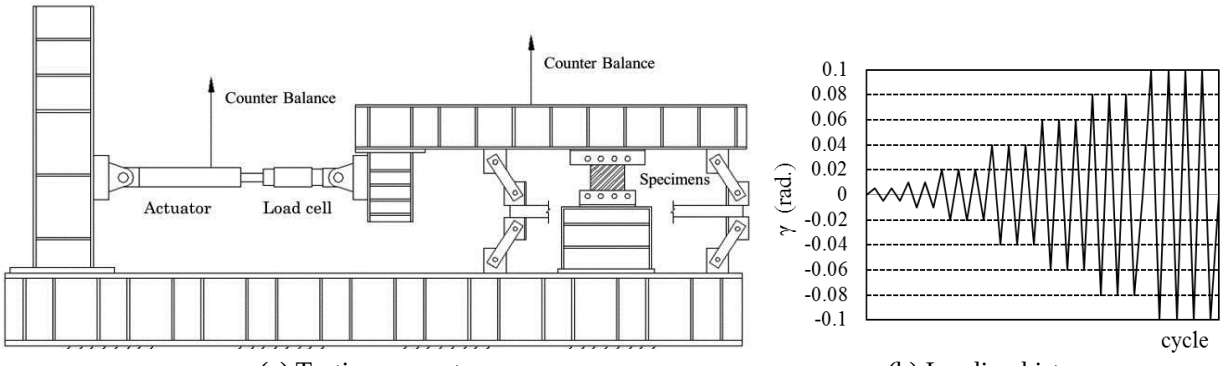

(a) Testing apparatus (b) Loading history

Figure 3. Details of testing method

3. TEST RESULTS AND DISCUSSION

3.1 Failure Mode

The photographs after tests of all eight test specimens are shown in Fig. 4. In case of specimens with one layer of CF sheet (see Fig. 4(a) and (e)), the out-of-plane deflections of the steel panels caused by premature shear buckling were obvious. And there is no remarkable crack in the steel panels of

specimen PB77-M20-1, while one crack was observed at the corner of steel panel of specimen PB55-M20-1. In both specimens, mortar plates damaged severely due to insufficient confinement. On the other hand, in case of specimens with two layers of CF sheet (see Figs. 4(b)-(d) and (f)-(h)), out-of-plane deflections of the steel panel caused by local buckling were concentrated at the corners of steel panel, and the center of steel panels remained plane till the end of tests. Magnitude of deflection of these specimens were small compared to those of the specimens with one layer of CF sheet, and the thicker the thickness of mortar plate the smaller the deflection. Significant cracks occurred at the corners of the panel due to fatigue under reversed cyclical loading. In these specimens, mortar plates were damaged in the upper and lower ends where steel panel locally buckled.

In all specimens, typical overall shear buckling and shear cracks at the center of the panel were not observed, which implies that the steel panel was effectively confined and prevented from premature out-of-plane bulking by the proposed confinement method. It is obvious that failure mode of all specimens is flexural-torsional buckling at corners.

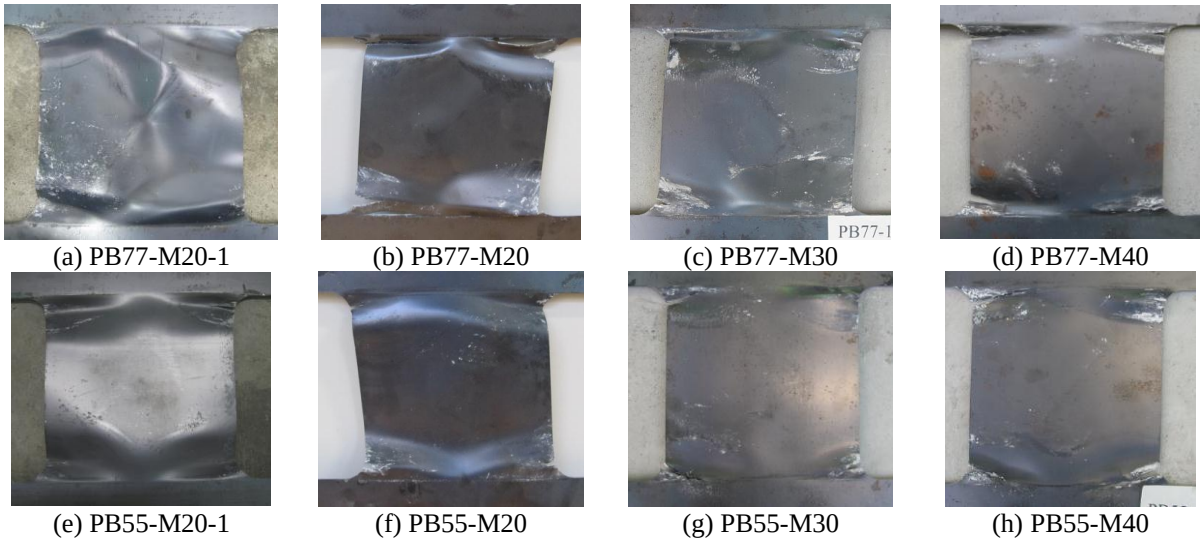

(a) PB77-M20-1 (b) PB77-M20 (c) PB77-M30 (d) PB77-M40

(e) PB55-M20-1 (f) PB55-M20 (g) PB55-M30 (h) PB55-M40

Figure 4. Failure modes of test specimens

3.2 Hysteretic Behavior

The measured shear force versus drift angle relationships of the test specimens are shown in Fig. 5. The circles marked in Fig. 5 represent ultimate shear force in both positive and negative directions. And the broken lines and solid lines superimposed express the theoretical yield shear forces ${}_{cal}Q_y$ and ultimate force ${}_{cal}Q_u$, respectively, which were calculated using the equations given in the next section. Comparisons of hysteresis loops at drift angle of 0.06rad are shown in Fig. 6. In the previous study on steel panels without confinement, shear forces reached the peak and decreased significantly at extremely small drift angles of no more than 0.01rad, before reaching their calculated yield shear capacities due to the premature shear buckling of steel panels (Zhang et al. 2008). All specimens expect for PB77-M20-1 kept spindle hysteretic loops and reached their ultimate strength at drift angle of 0.06rad, which verified effectiveness of the proposed method.

In both specimens with one layer of CF sheet (PB77-M20-1, PB55-M20-1), shear forces decreased immediately after reaching their calculated ultimate capacities and the strain hardening effect were little observed due to insufficient confinement by the CF sheet, and out-of-plane deflections increased (see Fig. 5(a) and (e)). These two specimens exhibited unstable energy-absorption capacities after ultimate strength, especially for PB77-M20-1. In case of specimens with two layers of CF sheet (see Figs. 5(b)-(d) and (f)-(h)), however the out-of-plane deflections of the specimens were minimal and the hysteretic loops remained stable until the tensile cracks occurred at the corners of the steel panels. The deterioration in shear force was primarily caused by the extension of cracks. In specimens with

width-thickness ratio of 55 and 77 with different mortar plate thickness, almost no difference on hysteretic performance was observed, until reaching their ultimate forces. Decrease in shear force occurred at the second cycle of 0.06rad for specimens with width-thickness ratio of 77 and second cycle of 0.08rad for specimens with width-thickness ratio of 55, due to the local bulking at the corners of the steel panels. As shown in Fig. 6, specimens with width-thickness ratio of 55 exhibited more stable hysteretic performance at a large drift angle of 0.06rad than specimens with width-thickness ratio of 77.

As shown in Fig. 5, the measured ultimate forces of all specimens were larger than the calculated results. From the viewpoint of safety margin, specimens with two layers of CF sheet and mortar plate thickness of over 20mm exhibited better hysteretic performance with spindle hysteretic loops, and are considered appropriate as a hysteretic damper.

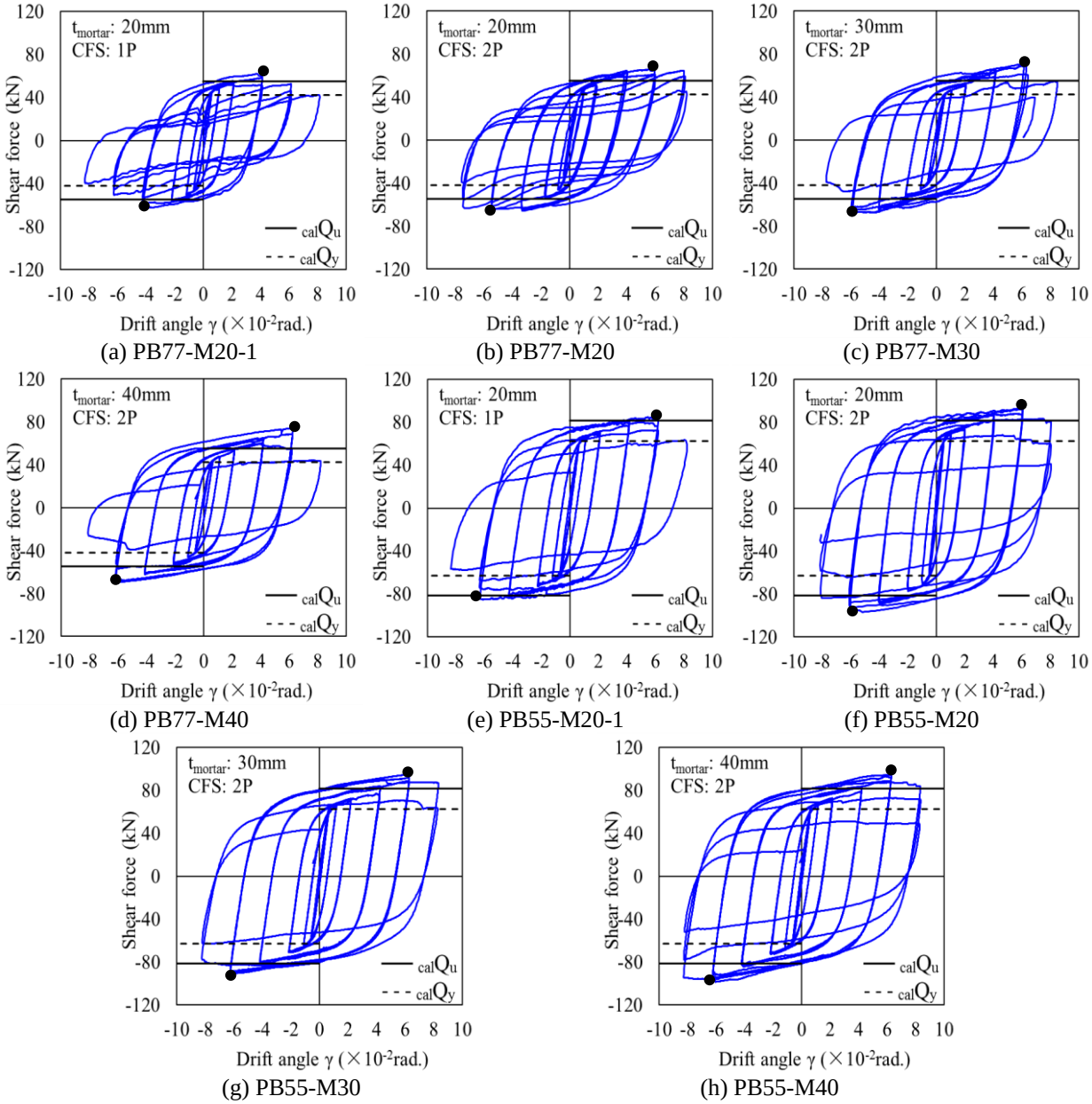

(a) PB77-M20-1 (b) PB77-M20 (c) PB77-M30

(d) PB77-M40 (e) PB55-M20-1 (f) PB55-M20

(g) PB55-M30 (h) PB55-M40

Figure 5. Measured shear force versus drift angle relationships

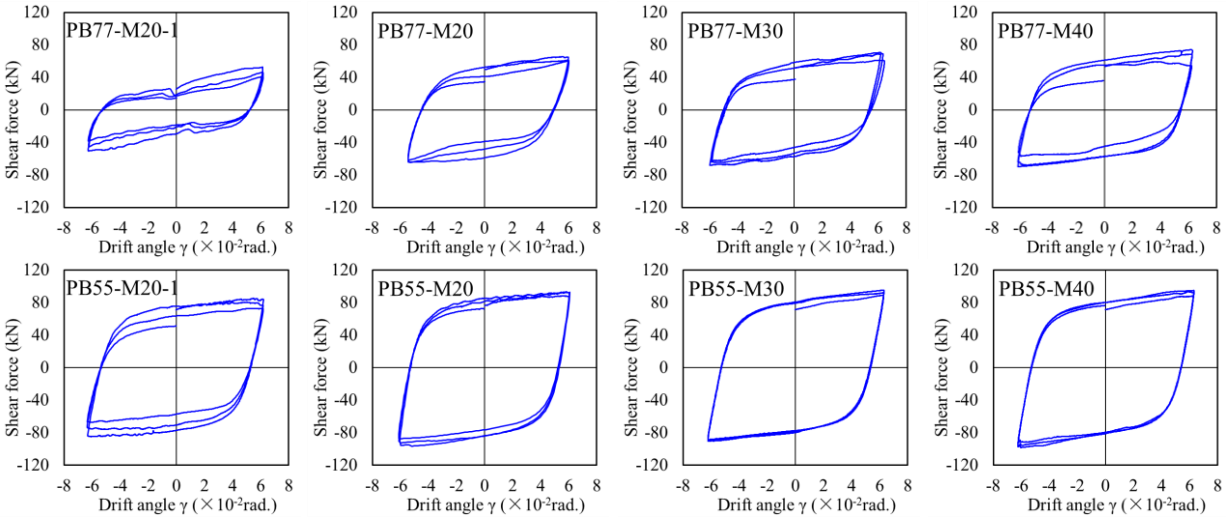

Figure 6. Measured shear force versus drift angle relationship at loop of γ=0.06 rad

4. EVALUATION OF STRENGTH AND STIFFNESS

The theoretical yield force of the specimen can be taken as the shear yield force of the steel panel, due to its pure shearing in small deformation. By assuming that shear stress across the steel panel section is distributed as shown in Fig. 7, the theoretical yield force ${}_{cal}Q_y$ can be calculated by Eqn. 4.1, where σ_y is the yield strength of the steel panel (N/mm^2), b and t are the width and thickness (mm), respectively.

$$ {}_{cal}Q_y = \frac{2}{3}\frac{\sigma_y}{\sqrt{3}}bt = \frac{2\sqrt{3}}{9}\sigma_y bt \tag{4.1} $$

Due to the flexural-torsional failure mode was observed eventually in all specimens, it is assumed that the theoretical ultimate force of the specimen can be taken as the flexural force of the steel panel corresponding to complete plastic moment. The theoretical ultimate force ${}_{cal}Q_u$ is given by Eqn. 4.2, which is derived by assuming the whole of cross section reaches the yield stress and the corresponding stress distribution is as shown in Fig. 8. In Eqn. 4.2, h is the height of the steel panel (mm).

$$ {}_{cal}Q_u = \frac{b^2 t}{2h}\sigma_y \tag{4.2} $$

The theoretical initial stiffness K_{cal} is obtained by Eqn. 4.3, simply adding the shear deformation to the flexural deformation of the steel panel. Due to the boundary conditions of bolts connection is not completely fixed, the height of steel panel h is modified as height h' when calculating the initial stiffness of specimens. The modified height h' is defined as the height between the centers of holes of the steel panel as shown in Fig. 9. In Eqn. 4.3, κ depends on the shape of the cross section, and equals to 1.2 for square section. E and G are Young's modulus and shear modulus of steel, respectively (N/mm^2).

$$ K_{cal} = \frac{1}{h^3 / Eb^3 t + \kappa h / Gbt} \tag{4.3} $$

The theoretical yield force, the ultimate force and the initial stiffness of specimens are summarized and compared with the experimental results in Table 4.1. As can be seen from Table 4.1, the measured yield forces of all specimens and the measured initial stiffness of specimens except for PB55-M20-1,

PB55-M30 and PB55-M40 were evaluated very well by using Eqn. 4.1 and Eqn. 4.2.

Theoretical predictions for ultimate strength of all specimens were smaller than the experimental results by approximately 4%-35%. It is presumed that strain hardening of steel led to the increase in strength.

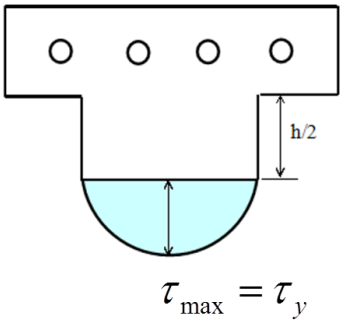

Figure 7. Distribution of shear stress at the yield force

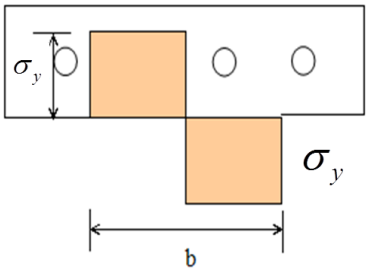

Figure 8. Distribution of shear stress at the ultimate force

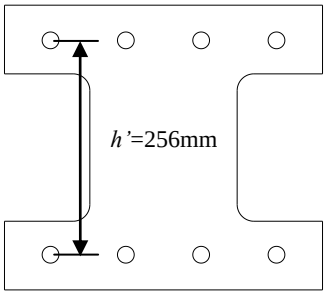

Figure 9. Definition of modified height *h'*

Table 4.1. Comparisons between the Measured Results and Theoretical Results

Specimen		Q_y	$_{cal}Q_y$	$Q_y/_{cal}Q_y$	Q_{max}	$_{cal}Q_u$	$Q_u/_{cal}Q_u$	K	K_{cal}	K/K_{cal}
PB77-M20-1	+	42.1	42.3	1.00	62.1	55.0	1.13	56.2	52.2	1.08
	-				62.4		1.13			
PB77-M20	+	45.8		1.08	65.4		1.19	56.0		1.07
	-				65.9		1.20			
PB77-M30	+	44.2		1.04	70.8		1.29	51.9		0.99
	-				68.1		1.24			
PB77-M40	+	44.4		1.05	74.2		1.35	56.7		1.08
	-				69.7		1.27			
PB55-M20-1	+	59.4	62.7	0.95	84.9	81.5	1.04	62.2	77.5	0.82
	-				85.2		1.05			
PB55-M20	+	69.4		1.11	93.1		1.14	82.7		1.07
	-				96.6		1.19			
PB55-M30	+	62.1		0.99	95.1		1.17	64.5		0.83
	-				90.5		1.11			
PB55-M40	+	64.2		1.02	94.7		1.16	66.0		0.85
	-				98.5		1.21			

5. MODELLING OF HYSTERETIC LOOPS

Skeleton-shift Model has been proposed by Meng et al. (1992) to describe strain hardening and Bauschinger effect of steel members, and it will be used to model the hysteretic behavior of specimens in this research. As shown in Fig. 10, the model consists of the skeleton curve composed of bi-linear curve, and hysteresis loops expressed by Ramberg-Osgood Model (Ramberg et al. 1943). Values of parameters for skeleton curve were determined by using the theoretical initial stiffness, yield shear strength and yield deformation, and values of parameters for Ramberg-Osgood curve were extracted from hysteresis loops of the specimens. Values of parameters used in this research are listed in Table 5.1.

Comparisons between the experimental and analytical hysteresis results of specimen PB77-M40 and PB55-M40 are shown in Fig. 11. Skeleton-shift Model traces the experimental results with reasonable accuracy. On the other hand, all specimens have common values of parameters for Ramberg-Osgood curve regardless of the width-thickness ratio; hence hysteresis can be conveniently modelled by using tensile test results for parameters of skeleton curve.

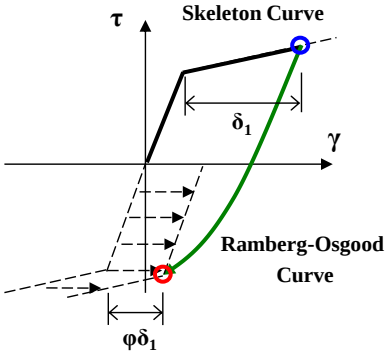

Figure 10. Skeleton-shift Model

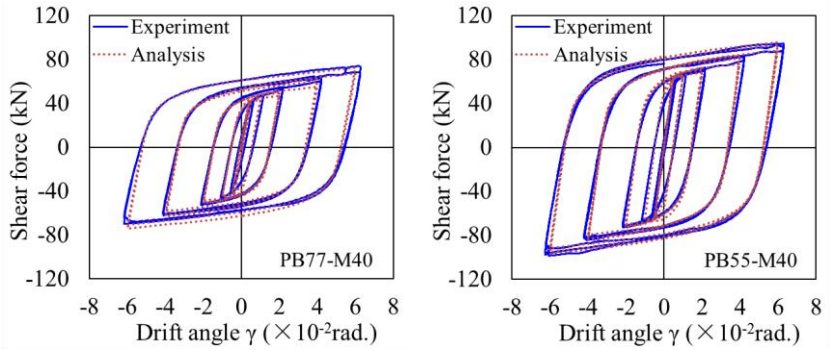

Figure 11. Comparison of hysteretic loops

Table 5.1. Values of Parameters Applied to the Skeleton-shift Model

Width-thickness Ratio	Skeleton Model				Ramberg-Osgood Model	
	Initial Stiffness	Strain Hardening Factor	Yield Strength	Yield Deformation	Shift Factor	Roundness Factor
77	53.0 kN/mm	0.020	42.3 kN	0.798 mm	0.7	11
55	71.4 kN/mm	0.015	62.7 kN	0.878 mm		

6. CONCLUSIONS

From the experimental and theoretical studies described in this paper, concluding remarks can be drawn as follows.

1) Confinement by mortar plates and CF sheets can prevent the steel panel from the premature shear buckling and make the steel panel an effective energy-absorption device.

2) Specimens with thickness of mortar plate over 20 mm and 2 layers of CF sheets exhibited better hysteretic performance. The out-of-plane deflections of these specimens were minimal and the hysteretic loops remained stable until the tensile cracks occurred at the corners of the steel panels.

3) The specimens with width-thickness ratio of about 55 showed more satisfactory hysteretic and energy dissipating performance than the specimens with width-thickness ratio of about 77.

4) The initial stiffness, yield force, ultimate force and hysteretic loops can be simply and accurately evaluated by using several concise equations and the Skeleton-shift Model, which implies that the proposed device can be simply designed and applied.

REFERENCES

Akiyama, H. (1985). Earthquake-resistant Limit-state Design of Buildings, University of Tokyo Press, Japan.

Tanaka, K. and Sasaki, Y. (1998). Study on Energy Absorbing Performance of Seismic Control Panel-damper Using Low-yield-point Steel under Static Loading, *Journal of Structural and Construction Engineering*, AIJ, No.509, 159-166. (in Japanese)

Tanaka, K., Sasaki, Y. and Yoneyama, S. (1999). An Experimental Study on Hysteretic Performance of Shear Panel Dampers Using Different Strength Type of Steel under Static Loading, *Journal of Structural and Construction Engineering*, AIJ, No.520, 117-124. (in Japanese)

Ikarashi, K., Shimizu, M. and Tomizawa, T. (2007). Cycle Characteristics of Thin Web Plate after Shear Buckling, *Journal of Structural and Construction Engineering*, AIJ, No.612, 197-205. (in Japanese)

Zhang, P., Sudo, T., Fujinaga, T. and Sun, Y. (2008). Energy Absorption Capacity of Steel Shear Panel Confined by Mortar Plates Wrapped with Carbon Fiber Sheet, *Steel Construction Engineering*, JSSC, Vol.15, No.60, 1-8. (in Japanese)

Meng, L., Ohi, K. and Takanashi, K. (1992). A Simplified Model of Steel Structural Members with Strength Deterioration Used for Earthquake Response Analysis, *Journal of Structural and Construction Engineering*, Architectural Institute of Japan, No. 437, 115-124. (in Japanese)

Ramberg, W. and Osgood, W. R. (1943). Description of stress-strain curves by three parameters, Technical Report No. 992, National Advisory Committee for Aeronautics Washington, D.C.